

Title:

Morphologically Engineered S-In_xZn_y Bimetallic Catalysts via an Ionothermal Approach for Enhanced Carbon Dioxide Electroreduction to Formate

Authors:

Xiaoyu Chen^a, Jie Liu^a, Shuoshuo Feng^a, Yanhong Zou^{b,*}, Kai Wu^c, Fanghua Ning^a, Jin Yi^a, Yuyu Liu^{a,*}

Affiliation:

^a Institute for Sustainable Energy, College of Sciences, Shanghai University, Baoshan District, Shanghai 200444, China.

^b School of Chemistry and Materials Engineering, Fuyang Normal University, 236037, China.

^c Nanotechnology Research Institute/G60 STI Valley Industry & Innovation Institute, College of Materials and Textile Engineering, Jiaxing University, Zhejiang, China.

*Corresponding authors

*E-mail addresses: yhzou@fynu.edu.cn (Yanhong Zou); liyuyuyu@shu.edu.cn, liyuyuyu2014@126.com (Yuyu Liu).

Content

Fig. S1. SEM image of In_2S_3 .

Fig. S2. SEM image of ZnS.

Fig. S3. Morphological evolution diagram of the catalysts (from $\text{In}_{3.5}\text{S}_1$ to $\text{In}_{0.2}\text{S}_1$).

Fig. S4. N_2 adsorption-desorption isotherms of (a) S- $\text{In}_{3.5}\text{Zn}_1$ catalyst, (b) In_2S_3 catalyst, (c) S- $\text{In}_{0.2}\text{Zn}_1$ catalyst, (d) S- $\text{In}_{0.5}\text{Zn}_1$ catalyst and (e) S- In_1Zn_1 catalyst.

Fig. S5. CV curves of (a) S- $\text{In}_{0.5}\text{Zn}_1$, (b) S- $\text{In}_{0.2}\text{Zn}_1$, (c) In_2S_3 , (d) S- $\text{In}_{3.5}\text{Zn}_1$ and (e) S- In_1Zn_1 catalysts in 0.5 M KHCO_3 solution under CO_2 -saturated atmosphere.

Fig. S6. CV curves of (a) S- $\text{In}_{3.5}\text{Zn}_1$, (b) In_2S_3 , (c) S- In_1Zn_1 , (d) S- $\text{In}_{0.2}\text{Zn}_1$ and (e) S- $\text{In}_{0.5}\text{Zn}_1$ catalysts in 0.5 M KHCO_3 solution under Ar-saturated atmosphere.

Fig. S7. The LSV curves of (a) In_2S_3 , (b) S- $\text{In}_{3.5}\text{Zn}_1$, (c) S- In_1Zn_1 , (d) S- $\text{In}_{0.2}\text{Zn}_1$ and (e) S- $\text{In}_{0.5}\text{Zn}_1$ in Ar and CO_2 -saturated 0.5 M KHCO_3 electrolyte.

Fig. S8. (a) $\text{FE}_{\text{CO}/\text{H}_2}$ diagram of In_2S_3 catalyst at different electrolysis potentials. (b) FE_{H_2} of four S- In_xZn_y catalysts at different electrolysis potentials.

Fig. S9. CV curves of the catalysts at different sweep speeds: (a) In_2S_3 catalyst, (b) S- $\text{In}_{3.5}\text{Zn}_1$ catalyst, (c) S- In_1Zn_1 catalyst, (d) S- $\text{In}_{0.5}\text{Zn}_1$ catalyst and (e) S- $\text{In}_{0.2}\text{Zn}_1$ catalyst.

Fig. S10. The partial current density of formate normalized by ECSA.

Table S1. Inductively Coupled Plasma Optical Emission Spectrometer (ICP-OES) results for mole ratio of In/Zn in different catalysts.

Table S2. Comparison of the performance of recently reported Indium based catalysts.

Table S3. Comparison of the ECO_2RR performance of In-based catalysts in flow cell.

Experiment section

Materials

Indium(III) nitrate hydrate ($\text{In}(\text{NO}_3)_3 \cdot x\text{H}_2\text{O}$, 99.99%), zinc acetate dihydrate ($\text{C}_4\text{H}_{10}\text{O}_6\text{Zn} \cdot 2\text{H}_2\text{O}$, 99%), and ethylene glycol ($\text{C}_2\text{H}_5\text{NS}$, $\geq 99.7\%$) were sourced from Shanghai Titan Scientific Co., Ltd. (China). Thioacetamide ($\text{C}_2\text{H}_6\text{O}_2$, $\geq 99.0\%$), potassium bicarbonate (KHCO_3 , 99.5%) and 5 wt% Nafion solution were procured from Sinopharm Chemical Reagent Co., Ltd. (China) and Shanghai Hesun Electrical Co., Ltd. (China), respectively. All chemicals were utilized without additional purification, with ultrapure water (18.2 $\text{M}\Omega \cdot \text{cm}$ resistivity) serving as the solvent throughout the experiments.

Preparation of the working electrodes

Carbon paper substrates ($2 \times 2 \text{ cm}^2$) were subjected to sequential ultrasonic cleaning in deionized water and ethanol, followed by vacuum drying. For catalyst ink preparation, 4 mg of the synthesized catalyst was dispersed in a mixture of 1 mL isopropanol and 40 μL Nafion solution (5 wt%) under 20-minute ultrasonication. The resulting homogeneous slurry was uniformly drop-casted onto the pretreated carbon paper, which subsequently served as the working electrode after ambient drying. The loading of the catalyst on the carbon paper was 1 mg cm^{-2} .

Synthesis of S- In_xZn_y

The preparation process of the catalyst involved the addition of a certain amount of indium nitrate, zinc acetate dihydrate, and thioacetamide into 20 mL of ethylene glycol. This mixture was stirred overnight and subsequently transferred into a 50 mL autoclave for a reaction at 160°C for six hours. After cooling to room temperature, the resultant solid was washed three times with water and ethanol, followed by vacuum drying at 60°C .

Synthesis of In_2S_3

In_2S_3 is synthesized using the same steps as S- In_xZn_y , except that no zinc acetate dihydrate is added during the synthesis process.

Characterization

The crystal structure was examined by X-ray diffraction (XRD, Rigaku

D/MAX2200V PC, Japan) with Cu-K α radiation ($\lambda = 1.5406 \text{ \AA}$). Morphological characterization was performed using scanning electron microscopy (SEM, JEOL JSM-7500F, Japan) and high-resolution transmission electron microscopy (HRTEM, JEOL JEM-F200, Japan) coupled with energy-dispersive X-ray spectroscopy (EDS). Surface chemical states were probed via X-ray photoelectron spectroscopy (XPS, Thermo Fisher ESCALAB 250Xi, UK). Specific surface area and pore size distribution were determined through Brunauer-Emmett-Teller (BET) analysis (Quantachrome Autosorb IQ2, USA) with N₂ adsorption-desorption isotherms. The metal content in the sample was analyzed via the inductively coupled plasma–optical emission spectroscopy (ICP-OES) technique (Agilent 5110, America).

Electrochemical measurements and product analysis

The electrocatalytic performance was characterized using a CHI760E electrochemical workstation. A conventional H-cell configuration was employed with 0.5 M KHCO₃ electrolyte, where the cathodic and anodic compartments were separated by a Nafion 117 ion-exchange membrane. A three-electrode system comprised a platinum plate counter electrode (2 × 2 cm), Ag/AgCl reference electrode, and working electrode. All measured potentials were converted to the reversible hydrogen electrode (RHE) scale according to the Nernst equation:

$$E_{RHE} = E_{Ag/AgCl} + E_{Ag/AgCl}^0 + 0.0591 \text{ pH} \quad (1)$$

where $E_{Ag/AgCl}^0$ is 0.199 V at 25°C.

Linear sweep voltammetry (LSV) measurements were performed at 50 mV s⁻¹ scan rate. To quantify the electrochemical active surface area (ECSA), cyclic voltammograms were recorded at varying scan rates (40 - 200 mV s⁻¹) within 0.23 to 0.04 V vs. RHE for electrochemical double-layer capacitance (C_{dl}) determination. Electrochemical impedance spectroscopy (EIS) was conducted over a frequency range of 10⁵ - 0.1 Hz.

The flow cell configuration consists of a gas diffusion electrode (GDE) (hydrophobically coated carbon paper as the gas diffusion layer and a carbon microporous layer as the catalyst) and a Pt sheet (1.5 cm × 3.5 cm, 1 mm thick) as the

cathode electrode and anode electrode, separated by an anion exchange membrane (Nafion 130), followed by a polytetrafluoroethylene (PTFE) spacer to position and sandwich the three components together. Ag/AgCl is used as the reference electrode. The catalyst was coated on a carbon microporous layer with a loading consistent with normal carbon paper of 1 mg cm⁻². The flow controller for CO₂ was controlled at 30 mL min⁻¹. In the flow cell, the electrolyte (1 M KOH) was circulated using a peristaltic pump (EC200-1, Wuhan Gaoss Union Technology Co., Ltd, Wuhan) with a silicone tube. Electrolyte flow was maintained at 25 mL min⁻¹. Electrochemical measurements and product analysis in the flow cell configuration were carried out by using the same electrochemical workstation and product analysis procedure as for the H-cell described above.

The concentration of the liquid-phase product was determined by using an ion chromatograph (IC1820, Sunny Hengping Scientific Instrument Co.). IC can qualitatively or quantitatively analyze anions and cations in liquid-phase products, and it has the advantages of high sensitivity and convenient operation. This study mainly utilizes it to determine the formate concentration. The concentration of gas-phase products was analyzed by online gas chromatography. The thermal conductivity detector (TCD) in the gas chromatograph (GC-2014C) equipped with an air generator and a hydrogen generator was mainly used to detect H₂, and the flame ionization detector (FID) was used to detect CO. The Faradaic efficiency (FE) for formate production was calculated as:

$$FE_{formate}(\%) = \frac{2 \times n \times F}{Q} \quad (2)$$

where n denotes moles of formate, Q represents total charge passed, and F is Faraday's constant (96,485 C mol⁻¹).

The FE values for gaseous products (H₂/CO) were determined through:

$$FE_{H_2/CO} = \frac{\frac{v}{60smin^{-1}} \times \frac{c}{2400cm^3mol^{-1}} \times N \times F}{j_{total}} \quad (3)$$

where v indicates gas flow rate (mL min⁻¹), c corresponds to gas concentration (vol%),

and N represents electron transfer number per molecule.

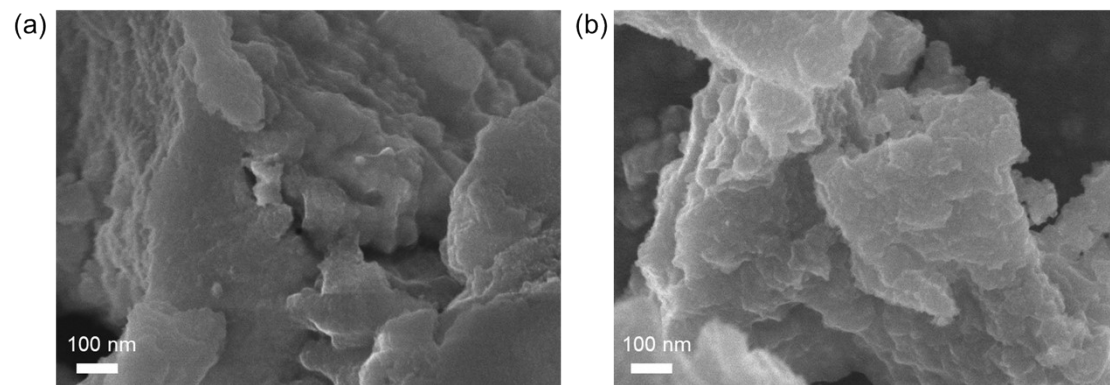


Fig. S1. SEM image of In_2S_3 .

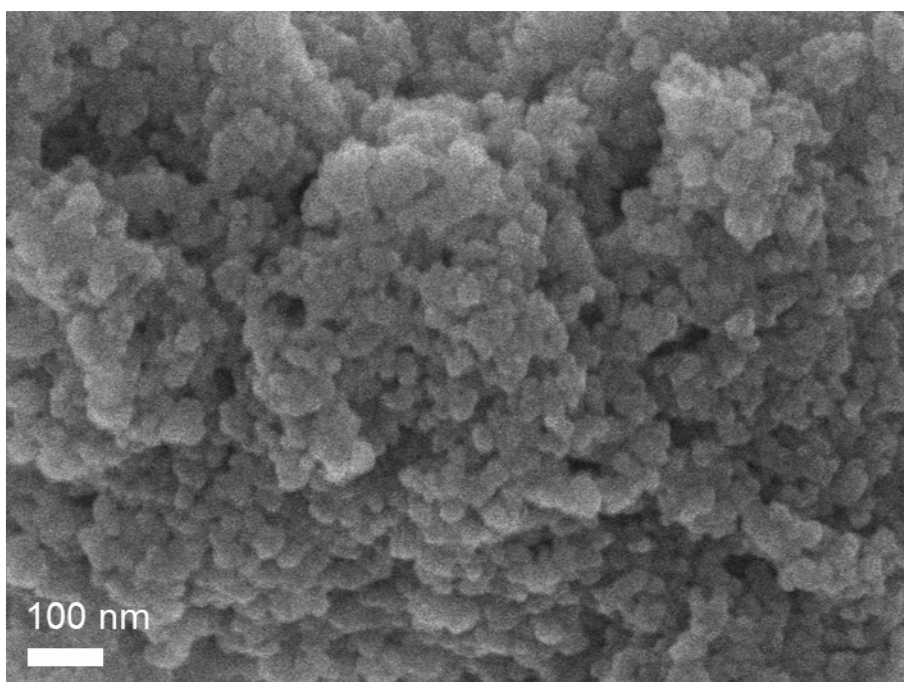


Fig. S2. SEM image of ZnS.

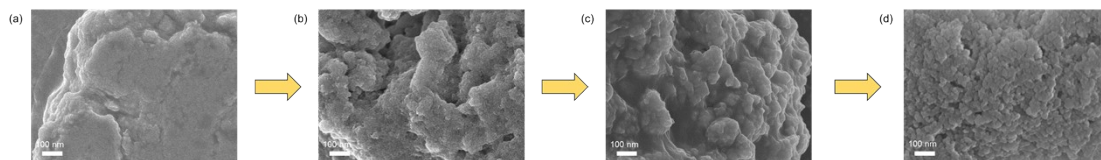


Fig. S3. Morphological evolution diagram of the catalysts (from $\text{In}_{3.5}\text{S}_1$ to $\text{In}_{0.2}\text{S}_1$).

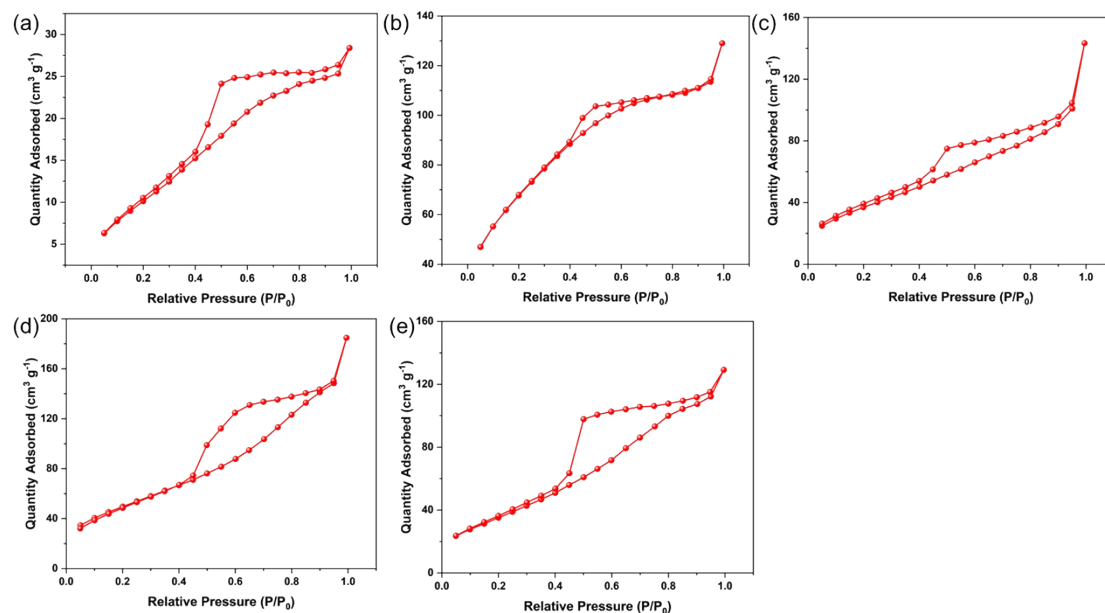


Fig. S4. N_2 adsorption-desorption isotherms of (a) S- $\text{In}_{3.5}\text{Zn}_1$ catalyst, (b) In_2S_3 catalyst, (c) S- $\text{In}_{0.2}\text{Zn}_1$ catalyst, (d) S- $\text{In}_{0.5}\text{Zn}_1$ catalyst and (e) S- In_1Zn_1 catalyst.

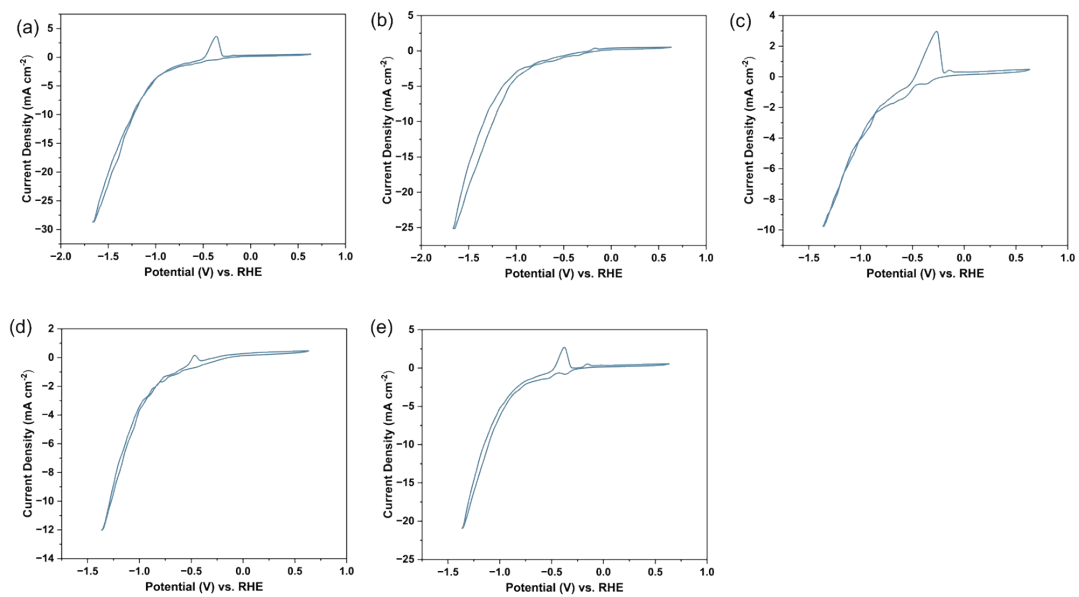


Fig. S5. CV curves of (a) S-In_{0.5}Zn₁, (b) S-In_{0.2}Zn₁, (c) In₂S₃, (d) S-In_{3.5}Zn₁ and (e) S-In₁Zn₁ catalysts in 0.5 M KHCO₃ solution under CO₂-saturated atmosphere.

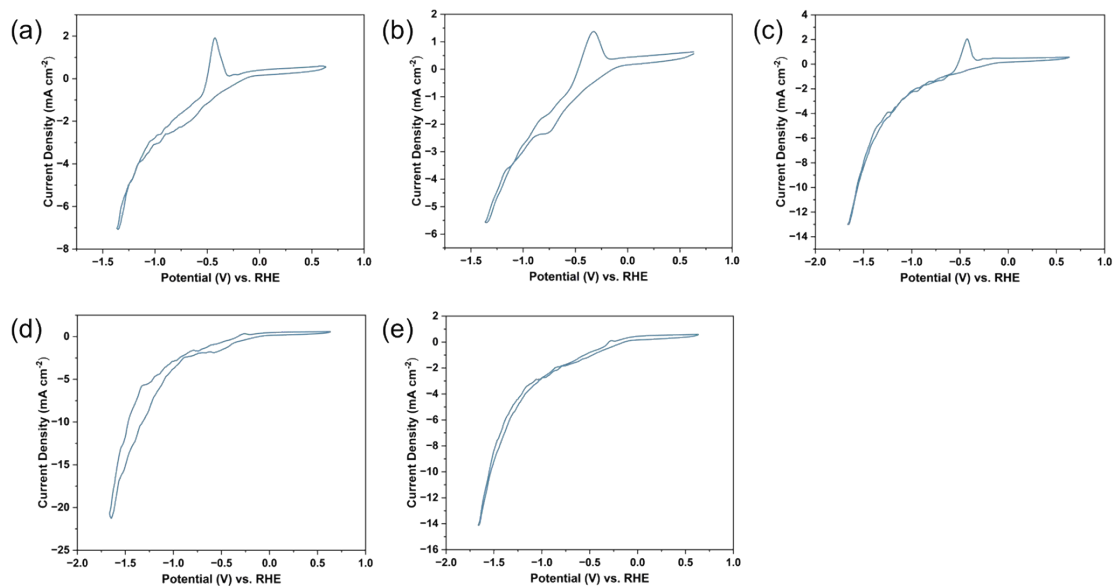


Fig. S6. CV curves of (a) S-In_{3.5}Zn₁, (b) In₂S₃, (c) S-In₁Zn₁, (d) S-In_{0.2}Zn₁ and (e) S-In_{0.5}Zn₁ catalysts in 0.5 M KHCO₃ solution under Ar-saturated atmosphere.

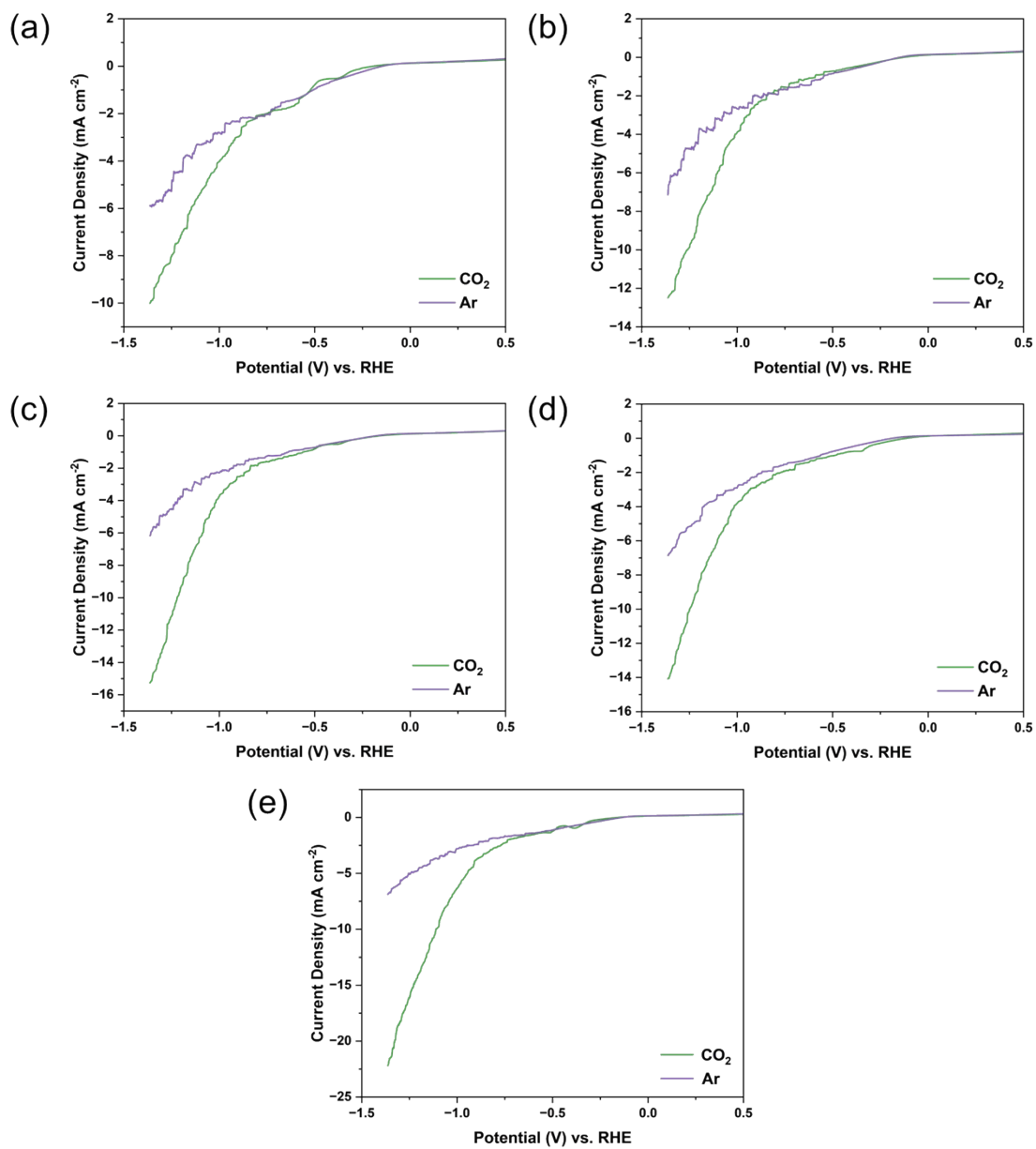


Fig. S7. The LSV curves of (a) In₂S₃, (b) S-In_{3.5}Zn₁, (c) S-In₁Zn₁, (d) S-In_{0.2}Zn₁ and (e) S-In_{0.5}Zn₁ in Ar and CO₂-saturated 0.5 M KHCO₃ electrolyte.

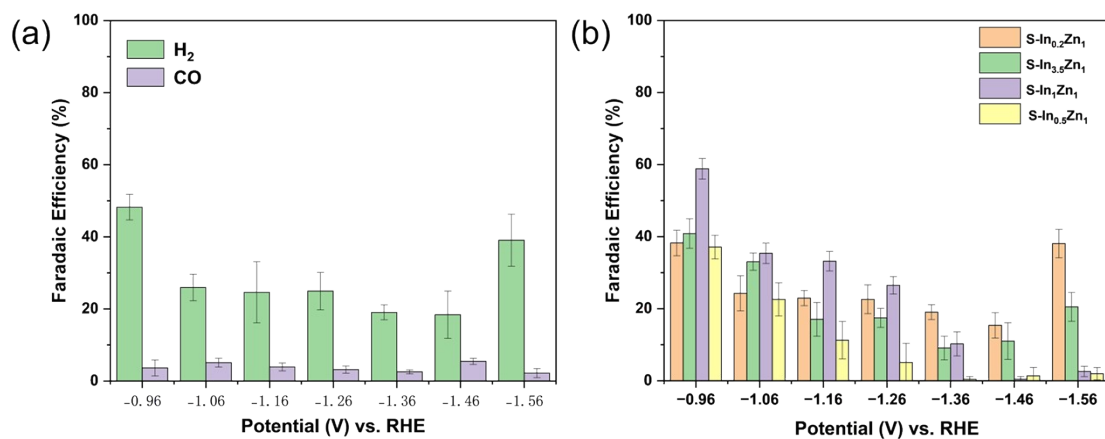


Fig. S8. (a) FE_{CO/H_2} diagram of In_2S_3 catalyst at different electrolysis potentials. (b) FE_{H_2} of four $S-In_xZn_y$ catalysts at different electrolysis potentials.

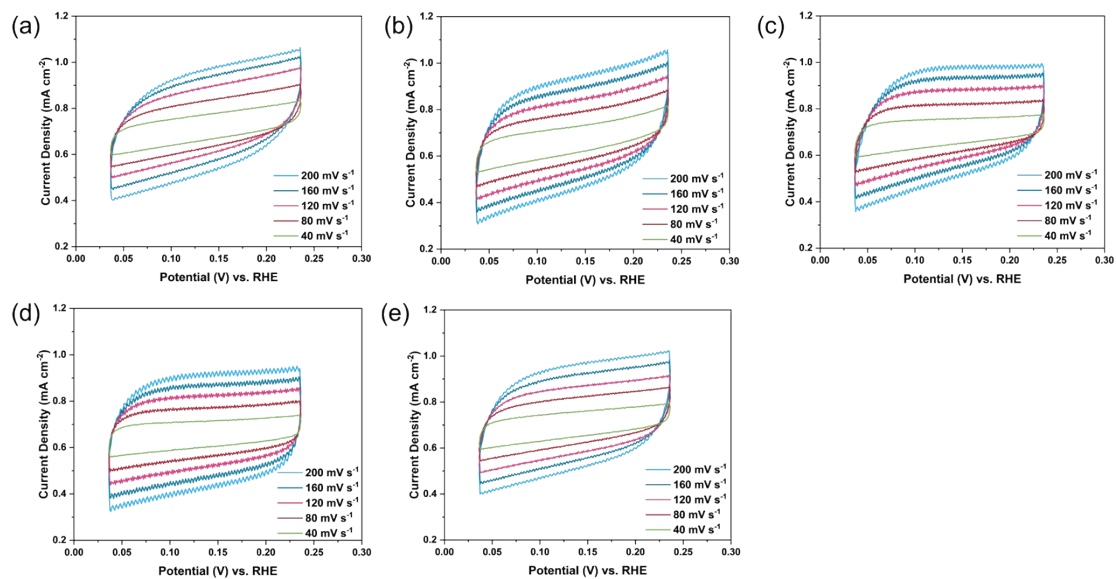


Fig. S9. CV curves of the catalysts at different sweep speeds: (a) In₂S₃ catalyst, (b) S-In_{3.5}Zn₁ catalyst, (c) S-In₁Zn₁ catalyst, (d) S-In_{0.5}Zn₁ catalyst and (e) S-In_{0.2}Zn₁ catalyst.

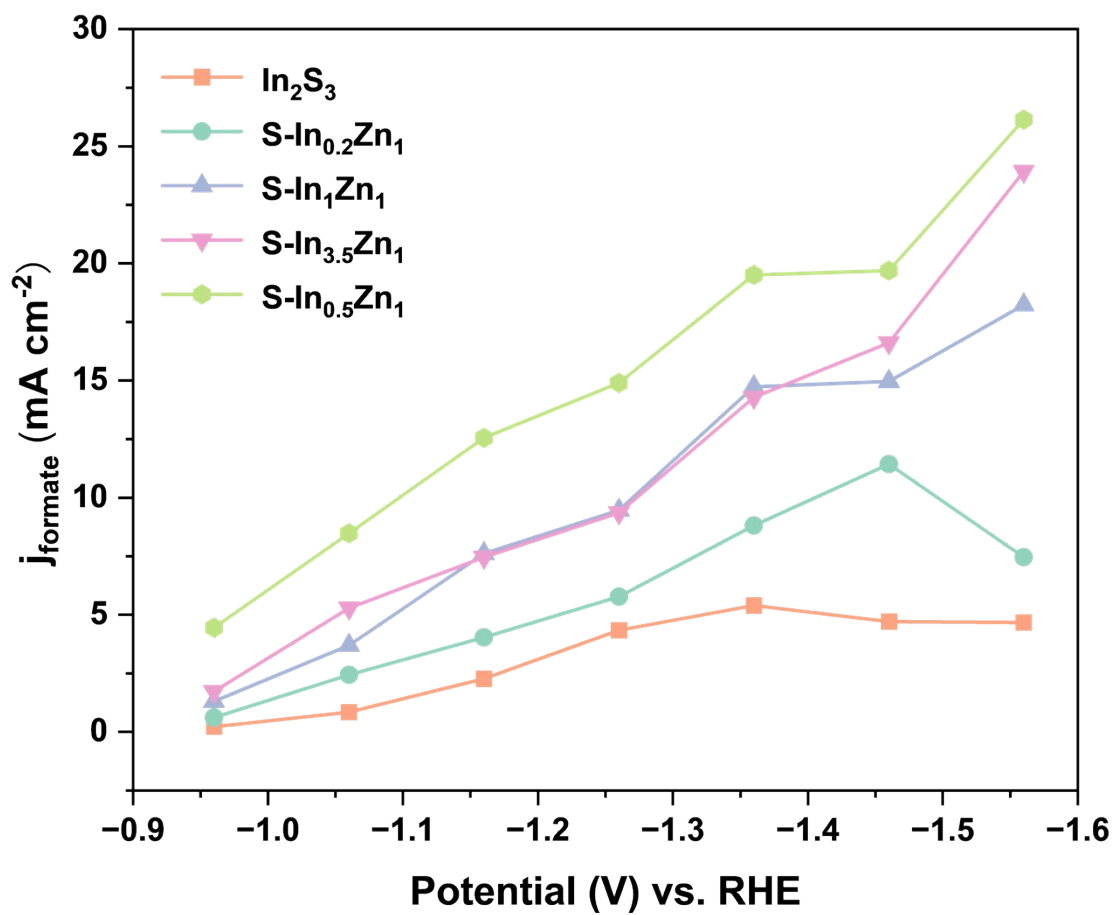


Fig. S10. The partial current density of formate normalized by ECSA.

Table S1. Inductively Coupled Plasma Optical Emission Spectrometer (ICP-OES) results for mole ratio of In/Zn in different catalysts.

Sample	ICP-OES (mole ratio, In/Zn)
S-In _{3.5} Zn ₁ catalyst	3.54
S-In ₁ Zn ₁ catalyst	0.93
S-In _{0.5} Zn ₁ catalyst	0.48
S-In _{0.2} Zn ₁ catalyst	0.22

Table S2. Comparison of the performance of recently reported Indium based catalysts.

Catalysts	Electrolyte	j_{formate} (mA cm ⁻²)	Production rate (μmol cm ⁻² h ⁻¹)	FE _{formate} (%)	Ref.
In-SAS/NC	0.5 M KHCO ₃	8.52	158	96	1
Hp-In	0.1 M KHCO ₃	60.75	1140	90.4	2
S-In ₂ O ₃	0.5 M KHCO ₃	53.1	1002	93	3
Mn doped In ₂ S ₃	0.1 M KHCO ₃	17.3	322	86	4
In-In ₂ S ₃	1.0 M KHCO ₃	20.9	752	76	5
Zn _{0.95} In _{0.05}	0.5 M KHCO ₃	14	400	95	6
ZnInO _x /NCF	0.5 M KHCO ₃	40.3	261	90.5	7

Table S3. Comparison of the ECO₂RR performance of Indium based catalysts in flow cell.

Catalysts	Electrolyte	Potential (V)	j_{total} (mA cm ⁻²)	FE _{formate} (%)	Ref.
In nanocrystals	1 M KOH	-1.4	150	70	8
In ₂ O ₃ @CNR	1 M KOH	-0.65	120	90.5	9
In ₂ O ₃ @C	1 M KOH	-1.4	185	93.5	10
In ₂ O ₃ nanosheets	1 M KOH	-0.59	322	86	11
In ₁ /S ₂	1 M KOH	-1.41	500	86.9	12
In/In ₂ O ₃ Ho-nt	1 M KOH	-1.0	386	93	13
Ni-In ₂ O ₃ @C NFs	1 M KOH	-1.0	396	90.5	14

Reference

1. H. Shang, T. Wang, J. Pei, Z. Jiang, D. Zhou, Y. Wang, H. Li, J. Dong, Z. Zhuang, W. Chen, D. Wang, J. Zhang and Y. Li, *Angew. Chem.-Int. Edit.*, 2020, **59**, 22465-22469.
2. W. Luo, W. Xie, M. Li, J. Zhang and A. Züttel, *J Mater Chem A*, 2019, **7**, 4505-4515.
3. W. Ma, S. Xie, X. Zhang, F. Sun, J. Kang, Z. Jiang, Q. Zhang, D. Wu and Y. Wang, *Nat. Commun.*, 2019, **10**, 892.
4. A. Zhang, Y. Liang, H. Li, X. Zhao, Y. Chen, B. Zhang, W. Zhu and J. Zeng, *Nano Lett.*, 2019, **19**, 6547-6553.
5. X. Yuan, Y. Luo, B. Zhang, C. Dong, J. Lei, F. Yi, T. Duan, W. Zhu and R. He, *Chem. Commun.*, 2020, **56**, 4212-4215.
6. I. S. Kwon, T. T. Debela, I. H. Kwak, H. W. Seo, K. Park, D. Kim, S. J. Yoo, J. Kim, J. Park and H. S. Kang, *J Mater Chem A*, 2019, **7**, 22879-22883.
7. X. Zhang, Z. Chen, M. Jiao, X. Ma, K. Mou, F. Cheng, Z. Wang, X. Zhang and L. Liu, *Appl. Catal. B-Environ.*, 2020, **279**, 119383.
8. Y. Zheng, P. Sun, S. Liu, W. Nie, H. Bao, L. Men, Q. Li, Z. Su, Y. Wan, C. Xia and H. Xie, *J. Colloid Interface Sci.*, 2025, **678**, 722-731.
9. B. Pan, G. Yuan, X. Zhao, N. Han, Y. Huang, K. Feng, C. Cheng, J. Zhong, L. Zhang, Y. Wang and Y. Li, *Small Sci.*, 2021, **1**, 2100029.
10. Z. Wang, Y. Zhou, D. Liu, R. Qi, C. Xia, M. Li, B. You and B. Y. Xia, *Angew. Chem.-Int. Edit.*, 2022, **61**, e202200552.
11. M. Jiang, M. Zhu, H. Wang, X. Song, J. Liang, D. Lin, C. Li, J. Cui, F. Li, X. L. Zhang, Z. Tie and Z. Jin, *Nano Letters*, 2023, **23**, 291-297.
12. T. Ma, F. Wang, W. Jing, H. Qiu, Y. Liu and L. Guo, *Adv. Funct. Mater.*, 2024, **34**, 2408977.
13. Z. Chen, D. Zhang, Y. Zhao, D. Jia, H. Zhang, L. Liu and X. He, *Chem. Eng. J.*, 2023, **464**, 142573.
14. Z. Chen, G. Yu, B. Li, X. Zhang, M. Jiao, N. Wang, X. Zhang and L. Liu, *ACS Catal.*, 2021, **11**, 14596-14604.

